第36卷第10期 无 机 化 学 学 报 Vol.36 No.10
2020年10月 CHINESE JOURNAL OF INORGANIC CHEMISTRY 1831-1844

三核和四核金属-有机簇修饰的四个多酸化合物的结构、选择性光催化和汞离子传感性能

应 俊 张宝月 田爱香*
(渤海大学化学系,锦州 121013)

摘要: 使用柔性含S有机配体4-(2-噻吩-2-基-乙基)-4*H*-[1,2,4]三氮唑(L),通过调控反应参数成功制备出4个基于Keggin的化合物,即[$Cu^{I}_{3}L_3(PMo_{12}O_{40})$] (**1**)、[$Cu^{I}_{4}L_6(SiW_{12}O_{40})$] (**2**)、[$Cu^{I}_{4}L_6(SiMo_{12}O_{40})$] (**3**)和[$Zn_4L_6(SiW_{12}O_{40})$] (**4**),并利用单晶X射线衍射、元素分析和红外光谱进行表征。化合物**1**中3个Cu^+离子聚合3个配体诱导一个环状的三核铜簇。Keggin多阴离子连接三核簇构筑二维层结构。化合物**2**、**3**和**4**同构,包含由6个配体连接4个金属离子(**2**、**3**中为铜离子,**4**中为锌离子)形成的四核$[M_4L_6]^{4+}$簇。多酸阴离子提供2个氧原子连接2个$[M_4L_6]^{4+}$簇,从而形成一维链结构。标题化合物对废水中的阳离子染料亚甲基蓝(MB)展示了良好的选择性光催化性能。另外**2**-CPE(碳糊电极)可作为安培传感器来检测过氧化氢和亚硝酸根。化合物**1**、**2**和**4**展示了对Hg^{2+}的传感性能。

关键词: 多酸基化合物; 电化学性能; 选择性光催化; Hg^{2+}传感
中图分类号: O614.121; O614.24+1 **文献标识码:** A **文章编号:** 1001-4861(2020)10-1831-14
DOI: 10.11862/CJIC.2020.218

Four Keggin Compounds Modified by Tri- and Tetra-nuclear Metal-Organic Clusters: Structures, Selective Photocatalytic and Hg^{2+} Recognition Characteristics

YING Jun ZHANG Bao-Yue TIAN Ai-Xiang*
(*Department of Chemistry, Bohai University, Jinzhou, Liaoning* 121013, *China*)

Abstract: By using a flexible S-containing ligand 4-(2-thiophen-2-yl-ethyl)-4*H*-[1,2,4]triazole (L), four Keggin-based compounds, namely [$Cu^{I}_{3}L_3(PMo_{12}O_{40})$] (**1**), [$Cu^{I}_{4}L_6(SiW_{12}O_{40})$] (**2**), [$Cu^{I}_{4}L_6(SiMo_{12}O_{40})$] (**3**) and [$Zn_4L_6(SiW_{12}O_{40})$] (**4**), were successfully synthesized by controlling the reaction parameters and well characterized by single-crystal X-ray diffraction, elemental analyses, and IR spectra. In compound **1**, three Cu^+ ions are fused by three L ligands inducing a cyclic tri-nuclear Cu^+ cluster. The Keggin anions link the tri-nuclear clusters to construct a 2D layer. Compounds **2**, **3** and **4** are isostructural, including a tetra-nuclear $[M_4L_6]^{4+}$ cluster with six L ligands connected by four M ions (M=Cu in **2** and **3**, Zn in **4**). The Keggin anion offers two O atoms to link two $[Cu_4L_6]^{4+}$ clusters and a 1D chain is formed. The title compounds exhibited good selective degradation of cationic methylene blue (MB) dye in wastewater. Additionally, the **2**-CPE (carbon paste electrodes) could act as an amperometric sensor for detection of hydrogen peroxide and nitrite. Compounds **1**, **2** and **4** also showed Hg^{2+} recognition properties. CCDC: 1879845, **1**; 1879846, **2**; 1879847, **3**; 1895379, **4**.

Keywords: polyoxometalate; electrochemical properties; selective photocatalysis; Hg^{2+} recognition

收稿日期:2020-03-15。收修改稿日期:2020-07-28。
国家自然科学基金(No.21571023,21101015)、辽宁省兴辽英才青年拔尖项目(No.XLYC1807049)和辽宁省教育厅项目(No.LQ2020010、LJ2019006)资助。
*通信联系人。E-mail:tian@bhu.edu.cn

0 Introduction

In the past few decades, polyoxometalates (POMs) have attracted significant attention because of their distinctive structures and extensive applications in catalysis[1-3], photo/electrochemistry[4-7], magnetism[8-10] and biochemistry[11-12]. The Keggin clusters as an essential part of the POM field possess unique basket-like structures. Up to now, it has been reported that a lot of Keggin-based compounds were modified by transition metal complexes (TMCs)[13]. In this work, we designed $[SiW/Mo_{12}O_{40}]^{4-}$, $[PMo_{12}O_{40}]^{3-}$ Keggin anions to construct POM-based compounds.

The organic ligands in TMCs play an important role for construction of Keggin-based compounds. At present, the N-donor containing ligands[14] are extensively used, containing rigid[15] and flexible types[16]. In our previous work, we usually used triazole and its derivatives to modify Keggin anions[17]. The triazole and its derivatives own many N donors to coordinate with TM ions. Namely, they can exhibit strong coordination abilities with TM ions. Furthermore, the concentrated N donors can induce interesting structures. For example, we have utilized the ligand 1-benzyl-1*H*-(1,3,4)triazole (3-btz) to construct a series of multi-nuclear metal-organic subunits, in order to modify POM anions[18]. Thus, in this work, we tried to design a new organic ligand with a triazole group, aiming to increase its coordination ability and modes. Moreover, in our previous work, we introduced S atom to organic amine, such as 2-(4-thiazolyl)benzimidazole (tba), aiming to explore new POM-based structures and appealing applications[19]. According to Pearson′s hard and soft acids and bases theory, soft Hg^{2+} ions (soft acid) can preferentially interact with sulfur (soft base). Thus, the introduction of S-containing ligands to POM-based series may construct new materials as fluorescent molecular probes for Hg^{2+}. Fortunately, a series of POM-based compounds modified by tba were obtained and they showed Hg^{2+} recognition properties. The Hg^{2+} is a well-known dangerous global pollutant. So it should be timely to detect Hg^{2+}[20]. Thus, the introduction of S to organic amines, especially the combination with triazole group, is a rational and appealing synthetic strategy to obtain new POM-based structures with good properties. In this work, we chose a new flexible S-containing ligand 4-(2-thiophen-2-yl-ethyl)-4*H*-[1,2,4] triazole (L) to modify POMs, which owns both a triazole group and a S-containing thiophen group. We want to use L to construct POM-based compounds owning not only new structures but also interesting properties of fluorescent molecular probes for Hg^{2+}.

Herein, we investigated the Keggin-Cu/Zn-L system to build four new Keggin-based compounds, $[Cu^{I}_{3}L_3(PMo_{12}O_{40})]$ (**1**), $[Cu^{I}_{4}L_6(SiW_{12}O_{40})]$ (**2**), $[Cu^{I}_{4}L_6(SiMo_{12}O_{40})]$ (**3**) and $[Zn_4L_6(SiW_{12}O_{40})]$ (**4**). Moreover, we have studied the amperometric sensing and photocatalytic properties under UV irradiation of compounds **1**~**4**. Compounds **1**, **2** and **4** can be used as chemosensors for detecting Hg^{2+}.

1 Experimental

1.1 Materials and general methods

All reagents were of analytical grade and were used as received from commercial sources without further purification. Elemental analyses (C, H and N) were performed on a Perkin-Elmer 240C CHN elemental analyzer, and the analyses of P, Cu, Mo, S, Si, W and Zn were carried out with a Leaman inductively coupled plasma (ICP) spectrometer. The IR spectra were got by a Magna FTIR 560 Spectrometer with KBr pellet in the 400~4 000 cm^{-1} region. Electrochemical measurements and data collection were performed with a CHI 660 electrochemical workstation. A conventional three-electrode system was used with a saturated calomel electrode (SCE) as reference electrode and a Pt wire as counter electrode. The carbon paste electrodes (CPEs) modified by the title compounds were used as the working electrodes. UV-Vis absorption spectra were obtained using a UV-1801 ultra violet spectrophotometer.

1.2 Syntheses of compounds 1~4

$[Cu^{I}_{3}L_3(PMo_{12}O_{40})]$ (**1**): A mixture of $H_3PMo_{12}O_{40}\cdot 6H_2O$ (0.08 g, 0.041 mmol), $Cu(CH_3COO)_2\cdot H_2O$ (0.1 g, 0.501 mmol) and L (0.02 g, 0.011 mmol) was dissolved in 10 mL of distilled water at room temperature. When

pH value of the mixture was adjusted to about 2.8 with 1.0 mol·L^{-1} HNO_3, the suspension was put into a Teflon-lined autoclave and kept under autogenous pressure at 160 ℃ for 4 d. After slow cooling to room temperature, dark red block crystals were filtered and washed with distilled water (Yield: 13% based on Mo). Anal. Calcd. for $C_{24}H_{27}N_9O_{40}S_3PMo_{12}Cu_3$(%): C, 11.30; H, 1.07; N, 4.94; Cu, 7.51; Mo, 45.12; P, 1.20; S, 3.81. Found(%): C, 12.25; H, 1.12; N, 4.88; Cu, 7.82; Mo, 46.25; P, 1.57; S, 4.04.

[$Cu^{I}_4L_6(SiW_{12}O_{40})$] (**2**): The synthesis of **2** was similar to **1** except that $H_4SiW_{12}O_{40}·26H_2O$ (0.08 g, 0.027 mmol) was used instead of $H_3PMo_{12}O_{40}$. When pH value of the mixture was adjusted to about 2.5 with 1.0 mol·L^{-1} HNO_3, the suspension was put into a Teflon-lined autoclave and kept under autogenous pressure at 170 ℃ for 4 d. After slow cooling to room temperature, red block crystals were filtered and washed with distilled water (Yield: 35% based on W). Anal. Calcd. for $C_{48}H_{54}N_{18}O_{40}S_6SiW_{12}Cu_4$(%): C, 13.71; H, 1.29; N, 6.00; Cu, 6.05; W, 52.48; Si, 0.67; S, 4.58. Found(%): C, 13.77; H, 1.33; N, 5.93; Cu, 5.98; W, 53.96; Si, 0.72; S, 4.32.

[$Cu^{I}_4L_6(SiMo_{12}O_{40})$] (**3**): The synthesis of **3** was the same as **2** except that $Na_2SiO_3·9H_2O$ (0.05 g, 0.17 mmol) and $Na_2MoO_4·2H_2O$ (0.1 g, 0.41 mmol) was used instead of $H_4SiW_{12}O_{40}·26H_2O$. Red block crystals were filtered and washed with distilled water (Yield: 27% based on Mo). Anal. Calcd. for $C_{48}H_{54}N_{18}O_{40}S_6SiMo_{12}Cu_4$ (%): C, 18.31; H, 1.73; N, 8.01; Cu, 8.07; Mo, 36.56; Si, 0.89; S, 6.11. Found(%): C, 18.37; H, 1.69; N, 7.92; Cu, 8.87; Mo, 37.02; Si, 0.97; S, 6.59.

[$Zn_4L_6(SiW_{12}O_{40})$] (**4**): The synthesis of **4** was the same as **2** except that $Zn(CH_3COO)_2·2H_2O$ (0.1 g, 0.46 mmol) was used instead of $Cu(CH_3COO)_2·H_2O$. Yellow block crystals were filtered and washed with distilled water (Yield: 30% based on W). Anal. Calcd. for $C_{48}H_{54}N_{18}O_{40}S_6SiW_{12}Zn_4$(%): C, 13.69; H, 1.29; N, 5.99; Zn, 6.21; W, 52.39; Si, 0.67; S, 4.57. Found(%): C, 13.61; H, 1.33; N, 5.92; Zn, 6.88; W, 52.10; Si, 0.61; S, 4.76.

1.3 Preparation of CPEs bulk-modified by compounds 1~4

CPE modified by compound **1** (**1**-CPE) was made as follows: 90 mg of graphite powder and 8 mg of **1** were mixed and ground together by an agate mortar and pestle to achieve a uniform mixture. And then 0.1 mL of Nujol was added with stirring. The homogenized mixture was packed into a glass tube with a 1.5 mm inner diameter, and the tube surface was wiped with weighing paper. Electrical contact was established with a copper rod through the back of the electrode. In a similar manner, **2**-, **3**- and **4**-CPEs were made with compounds **2**~**4**.

1.4 X-ray crystallographic study

X-ray diffraction analysis data for compounds **1**~**4** were collected with a Bruker Smart Apex CCD diffractometer using Mo $K\alpha$ radiation (λ =0.071 073 nm) at 293 K. All crystal structures were solved by direct methods and refined on F^2 by full-matrix least squares methods using the SHELX-97 package[21]. The structures were solved and refined using the OLEX2 program suite[22], equipped with the SHELXS and SHELXL programs. All the hydrogen atoms attached to carbon atoms were generated geometrically. The crystal data and structures refinement for **1**~**4** are given in Table 1. Selected bond lengths (nm) and angles (°) of **1**~**4** are listed in Table S1(Supporting information).

Table 1 Crystal data and structure refinement for compounds 1~4

Compound	1	2	3	4
Formula	$C_{24}H_{27}N_9O_{40}S_3PMo_{12}Cu_3$	$C_{48}H_{54}N_{18}O_{40}S_6SiW_{12}Cu_4$	$C_{48}H_{54}N_{18}O_{40}S_6SiMo_{12}Cu_4$	$C_{48}H_{54}N_{18}O_{40}S_6SiW_{12}Zn_4$
Formula weight	2 550.6	4 203.9	3 149.0	4 211.2
Crystal system	Triclinic	Monoclinic	Monoclinic	Monoclinic
Space group	$P\bar{1}$	$P2_1/n$	$P2_1/n$	$P2_1/n$
a / nm	1.411 1(2)	1.314 8(10)	1.313 5(11)	1.313 5(5)
b / nm	1.514 1(3)	1.505 8(11)	1.500 0(13)	1.504 1(6)
c / nm	1.552 6(3)	2.206 3(16)	2.201 7(18)	2.203 5(8)

Continued Table 1

α / (°)	64.127(3)			
β / (°)	85.207(3)	92.914(2)	93.15(2)	92.95(10)
γ / (°)	74.353(3)			
V / nm^3	2.871 7(8)	4.362 3(6)	4.331 6(6)	4.347 5(3)
Z	2	2	2	2
D_c / (g·cm^{-3})	2.950	3.200	2.414	3.217
μ / mm^{-1}	3.852	16.948	2.884	17.131
F(000)	2 416	3 804	3 036	3 812
Reflection collected	20 683	27 150	30 639	31 478
Independent reflection	13 956	8 676	10 230	10 702
R_{int}	0.047 9	0.070 4	0.058 7	0.055 2
Reflection [$I>2\sigma(I)$]	8 468	5 708	6 188	7 601
R_1[a] [$I>2\sigma(I)$]	0.060 5	0.047 0	0.071 0	0.044 6
wR_2[b] (all data)	0.156 3	0.100 9	0.147 0	0.099 1
GOF on F^2	0.987	1.009	1.022	1.025

[a] $R_1=\sum||F_o|-|F_c||/\sum|F_o|$; [b] $wR_2=\{\sum[w(F_o^2-F_c^2)^2]/\sum[w(F_o^2)^2]\}^{1/2}$.

In the process of refinement, due to the vibration of Mo-O and W-O bond, the thermal ellipsoid of O atom was elongated. So, these O atoms were refined according to the disorder model. At the same time, the thermal ellipsoid of the C-S chain on the ligand was obviously enlarged due to the rotation of the single bond, and these atoms were also refined according to the disorder model. It was found that RIGU and ISOR instructions need to be added, and good results could be obtained. Therefore, we have added some necessary restrictions to the models of compounds **1**~**4**, which made it easier for us to get a better model of the compounds.

2 Results and discussion

2.1 Description of crystal structures

2.1.1 Crystal structure of compound **1**

Crystal structure analysis reveals that compound **1** consists of three Cu(I) ions, three L ligands, one $[PMo_{12}O_{40}]^{3-}$ (abbreviated to PMo_{12}) anion (Fig. 1). The valence sum calculations show that all the Mo atoms in **1**, **3** and all the W atoms in **2** are in +6 oxidation states. Four of the twelve W atoms in **4** are in +5 oxidation states. All the Cu ions in **1**~**3** are in +1 oxidation state, and the Zn ion in **4** is in +2 oxidation states[23]. The oxidation state of Cu ions in **1**~**3** are +1, although the starting material was $Cu(CH_3COO)_2\cdot H_2O$ with +2 oxidation state. The reason is that N-containing organic ligands can act as not only organic ligands, but also reducing agents to reduce the oxidation state of copper from +2 to +1 under hydrothermal conditions[24-25].

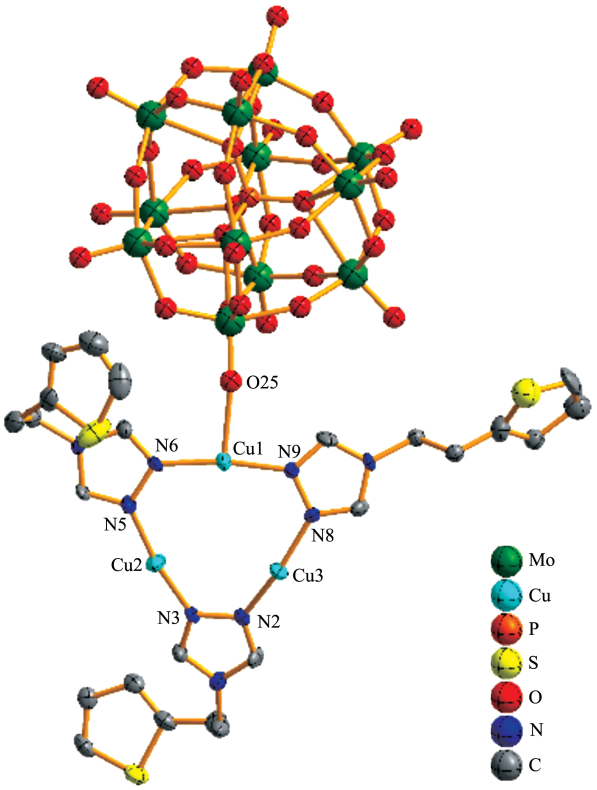

Thermal ellipsoids are drawn at 50% probability level; Hydrogen atoms are omitted for clarity

Fig.1 Ellipsoids view of asymmetric unit of **1**

In compound **1**, there exist three crystallographically independent Cu(I) ions (Cu1, Cu2 and Cu3), showing two kinds of coordination modes. The Cu1 is three-coordinated by two N atoms (N6 and N9) from two L ligands and one terminal O25 from one PMo_{12} anion. The Cu2 ion is three-coordinated by two N donors (N3 and N5) from two L ligands and one terminal O31 from one PMo_{12} anion. The Cu3 ion is four-coordinated by two N atoms (N2 and N8) from two L ligands and two terminal oxygen atoms O6 and O13 from two PMo_{12} anions. The Cu-N distances are in a range of 0.189 5(9)~0.190 9(8) nm, while the Cu-O bonds are from 0.228 9(7) to 0.241 6(7) nm. The N-Cu-N angles are in a range of 163.9(4)°~170.4(4)°, while the O-Cu-N angles are from 91.7(3)° to 100.8(3)° (Table S1). The bond distances and angles in **1** are comparable to those in the similar Cu(I) coordination modes.

In compound **1**, the S atom in thiophen group is uncoordinated with Cu(I) ions. Each L ligand provides two N to link two different Cu ions, and a cyclic trinuclear copper cluster was induced using the characteristic of triazole group (Fig.S1). Each PMo_{12} provides 4 terminal oxygen (O6, O13, O25 and O31) to connect four Cu ions from four tri-nuclear cycles. Each tri-nuclear Cu(I) cycle offers two copper atoms to link two Keggin anions, while the third copper atom connects two anions. The coordination modes of the Keggin anion and the tri-nuclear Cu(I) cluster induce a 2D layer of compound **1**, as shown in Fig.2 (top) and Fig.S2. Because each Keggin anion links four tri-nuclear Cu(I) cycles and each tri-nuclear cycle connects four Keggin anions, the Keggin anion and tri-nuclear cycle can be used as four connected nodes respectively. Thus, the simplified topology of 2D layer of compound **1** is shown in Fig.2 (bottom).

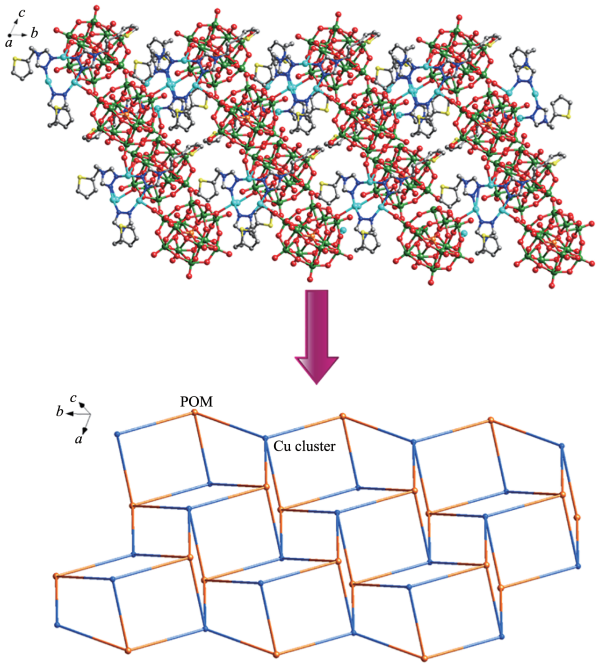

Fig.2　Top: 2D layer of compound 1 with tri-nuclear Cu(I) cycles linked by PMo_{12} anions; Bottom: simplified topology of 2D layer in compound **1** with the Keggin anions (orange balls) and tri-nuclear cycles (blue balls) as four connected nodes, respectively

2.1.2　Crystal structure of compound **2**

Crystal structure analysis reveals that compound **2** consists of four Cu(I) ions, six L ligands, and one $[SiW_{12}O_{40}]^{4-}$ anion (abbreviated to SiW_{12}) (Fig.3).

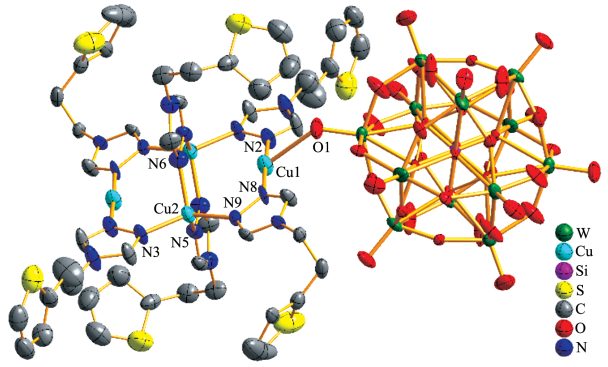

Thermal ellipsoids are drawn at 50% probability level; Hydrogen atoms are omitted for clarity

Fig.3　Ellipsoids view of asymmetric unit of **2**

In compound **2**, there are two crystallographically independent Cu(I) ions (Cu1 and Cu2), showing two kinds of coordination geometries. The Cu1 exhibits a distorted trigonal planar configuration, three-coordinated by two N donors (N2 and N8) from two L ligands and one O1 from one anion. The Cu-N bond distances are in a range of 0.190 5(10)~0.191 4(11) nm and N-Cu-N angle is 175.6(6)°. The Cu2 ion is four-coordinated by four N atoms (N3, N5, N6 and N9) from four L ligands, exhibiting a distorted tetrahedron. Around the Cu2 ion, the Cu-N bond distances are in a range of 0.200 2(11)~0.206 6(12) nm, while the N-Cu-N angles are from

100.4(5)° to 124.9(4)° (Table S1). The bond distances and angles of Cu(I) are similar to that in compound **1**. In compound **2**, the L ligand also uses its two apical N donors to fuse Cu(I) ions. Firstly, four L molecules are linked by four Cu ions to construct a tetra- nuclear planar rectangle cluster. Furthermore, the other two L ligands cover this rectangle up and down. These two ligands are vertical with the planar rectangle cluster. The tetra-nuclear Cu cluster is formulated as $[Cu_4L_6]^{4+}$ (Fig. S3). The SiW_{12} anion provides two terminal O atoms to connect two tetra-nuclear Cu clusters $[Cu_4L_6]^{4+}$. Thus, a chain of **2** is formed with SiW_{12} anions and $[Cu_4L_6]^{4+}$ clusters arranging alternately (Fig. 4). The adjacent chains link each other through hydrogen bonding interactions to build a 2D supramolecular structure of **2** (Fig.S4).

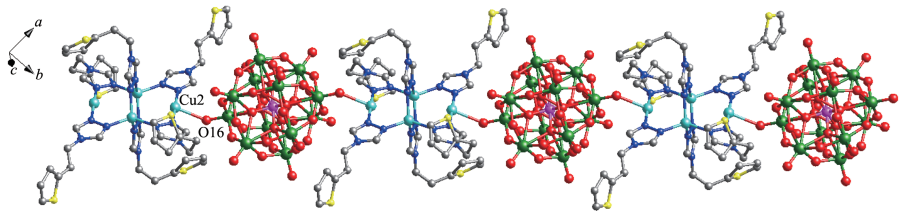

Fig.4 One-dimensional chain of compound **2** with SiW_{12} anions and $[Cu_4L_6]^{4+}$ clusters arranging alternately

2.1.3 Crystal structure of compounds **3** and **4**

Crystal structure analysis reveals that compound **3** is isostructural with **2**, consisting of four Cu(I) ions, six L ligands, and one $[SiMo_{12}O_{40}]^{4-}$ anion (abbreviated to $SiMo_{12}$) (Fig.S5). In compound **3**, there are two crystallographically independent Cu(I) ions (Cu1 and Cu2). The Cu1 ion is three-coordinated by two N donors (N3 and N4) from two L ligands and one O1 from $SiMo_{12}$ anion. The Cu2 ion is four-coordinated by four N atoms (N2, N5, N7 and N4) from four L ligands and one O1 from one anion. Around the Cu ion, the Cu-N bond distances are in a range of 0.189 8(8)~0.206 8(8) nm, while the Cu-O distance is 0.248 6(7) nm. The N-Cu-N angles are from 99.6(3)° to 176.3(4)° (Table S1).

Crystal structure analysis reveals that compound **4** is isostructural with **2** and **3**, consisting of four Zn(Ⅱ) ions, six L ligands, and one $[SiW_{12}O_{40}]^{4-}$ anion (abbreviated to SiW_{12}). In compound **4**, there are two crystallographically independent Zn(Ⅱ) ions (Zn1 and Zn2). The Zn1 is four-coordinated by four N donors (N2, N3, N5 and N8) from four L ligands. The Zn2 ion is three-coordinated by two N atoms (N6 and N9) from two L ligands and one O1 from one anion. Around the Zn ion, the Zn-N bond distances are in a range of 0.190 4(7)~0.206 9(7) nm, while the Zn-O distance is 0.2489(7) nm. The N-Zn-N angles are from 99.6(3)° to 175.5(4)° (Table S1).

2.2 FT-IR spectra

Fig.S6 shows the IR spectra of L ligand and compounds **1**~**4**. In the spectrum, characteristic bands at 1 060, 958, 873 and 798 cm^{-1} for **1** are attributed to ν(P-O_a), ν(Mo-O_t), ν(Mo-$O_{b/c}$-Mo). Characteristic bands at 968, 920, 881 and 792 cm^{-1} for **2** and 967, 919, 877 and 798 cm^{-1} for **4** are attributed to ν(Si-O_a), ν(W-O_t), ν(W-$O_{b/c}$-W). Characteristic bands at 949, 900, 859 and 794 cm^{-1} for **3** are attributed to ν(Si-O_a), ν(Mo-O_t), ν(Mo-$O_{b/c}$-Mo)[26]. Bands in the regions of 1 654~1 199 cm^{-1} for **1**, 1 625~1 192 cm^{-1} for **2**, 1 637~1 194 cm^{-1} for **3**, 1 685~1 193 cm^{-1} for **4** are attributed to the L ligand, respectively.

2.3 Electrochemical properties

We have studied the electrochemical properties of compounds **1**~**4** in 0.1 mol·L^{-1} H_2SO_4+0.5 mol·L^{-1} Na_2SO_4 aqueous solution. Owing to the similar electrochemical behaviors of **1**- and **3**-CPEs and **2**- and **4**-CPEs, **1**- and **2**-CPEs were chosen as examples. The cyclic voltammograms for the **1**-CPE in 0.1 mol·L^{-1} H_2SO_4+0.5 mol·L^{-1} Na_2SO_4 aqueous solution at different scan rates are shown in Fig. 5. In the potential range of 600~−260 mV, there were three reversible redox peaks Ⅰ-Ⅰ′, Ⅱ-Ⅱ′ and Ⅲ-Ⅲ′, with the half-wave potentials ($E_{1/2}$=(E_{pa}+E_{pc})/2) of 299 mV (Ⅰ-Ⅰ′), 160 mV (Ⅱ-Ⅱ′) and −80 mV (Ⅲ-Ⅲ′) (Scan rate: 60 mV·s^{-1}). Redox peaks Ⅰ-Ⅰ′, Ⅱ-Ⅱ′ and Ⅲ-Ⅲ′ corre-

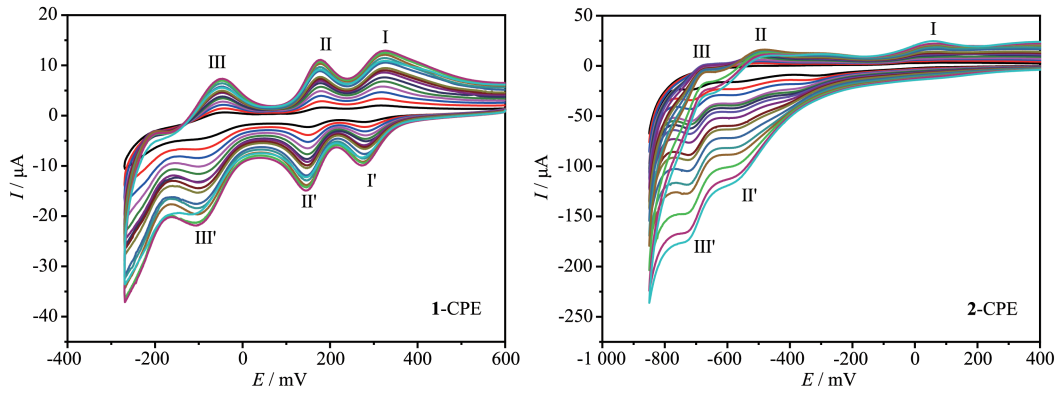

From inner to outer: 20, 40, 60, 80, 100, 120, 140, 160, 180, 200, 250, 300, 350, 400, 450 and 500 mV·s^{-1}, respectively

Fig.5　Cyclic voltammograms of **1**- and **2**-CPEs in 0.1 mol·L^{-1} H_2SO_4 + 0.5 mol·L^{-1} Na_2SO_4 aqueous solution at different scan rates

spond to three consecutive two-electron processes of PMo_{12}[27]. The cyclic voltammograms of **2**-CPE at different scan rates are presented in the potential range of 400~-850 mV. There were two reversible redox peaks Ⅱ-Ⅱ′ and Ⅲ-Ⅲ′ with the half-wave potentials of −510 and −711 mV (Scan rate: 60 mV·s^{-1}), corresponding to two consecutive two-electron processes of SiW_{12}[28]. Moreover, there was also one irreversible anodic peak Ⅰ with the potential of 50 mV, which is assigned to the oxidation of the copper centers. The redox peaks for heteropoly molybdate-based **1**-CPE appeared at or near positive potential, while the redox peaks for heteropoly tungstate-based **2**-CPE appeared at negative potential. Furthermore, the irreversible anodic peak for oxidation of the copper center appeared in **2**-CPE but was overlapped in **1**-CPE. The peak potentials changed gradually from 20 to 500 mV·s^{-1} of scan rates. The cathodic peak potentials shifted towards the negative direction, while the corresponding anodic peak potentials to the positive direction.

Fig.S7 shows cyclic voltammograms for the electrocatalytic reduction of NO_2^- at **1**- and **2**-CPEs. With the addition of NO_2^-, all the reduction peak currents increased remarkably, while the corresponding oxidation peak currents gradually decreased. These phenomena show that all the reductive species of PMo_{12} and SiW_{12} possess electrocatalytic activities for the reduction of NO_2^-. As shown in Fig.S7, when bromate was added in the aqueous solution, we could clearly observe that the second and the third reduction peak currents for **1**-CPE and all the reduction peak currents for **2**-CPE gradually increased and the corresponding oxidation peak currents visibly decreased. However, the first redox peak of **1**-CPE remained almost unchanged, showing that the bromate is reduced only by four- and six-electron reduced species of PMo_{12} in **1**-CPE. When we added hydrogen peroxide in the aqueous solution, the second and the third reduction peak currents for **1**-CPE and all the reduction peak currents for **2**-CPE gradually increased and the corresponding oxidation peak currents visibly decreased (Fig.S7). In a word, **1**- and **2**-CPEs exhibit good electrocatalytic activities for the reduction of nitrite, bromate and hydrogen peroxide.

2.4　2-CPE as an amperometric sensor

In this work, we used the **2**-CPE as a hydrogen peroxide and nitrite amperometric sensor, respectively[29]. We added hydrogen peroxide and nitrite successively to continuously stirred 0.1 mol·L^{-1} H_2SO_4+0.5 mol·L^{-1} Na_2SO_4 aqueous solution to obtain the **2**-CPE typical hydrodynamic amperometry, as shown in Fig.6. The **2**-CPE electrode response time for hydrogen peroxide reduction was 3.6 s. Fig.6b shows the calibration graph at the **2**-CPE. The electrode response was linear for hydrogen peroxide within the concentration range of 2~9.2 mmol·L^{-1}, and the sensitivity was 0.28 μA·L·mmol^{-1} (Correlation coefficient: 0.998 66). The detection limit was 0.282 mmol·L^{-1} when the signal-to-noise ratio was 3. The **2**-CPE electrode response time for nitrite reduction was 4.5 s. Fig.6d shows the calibration

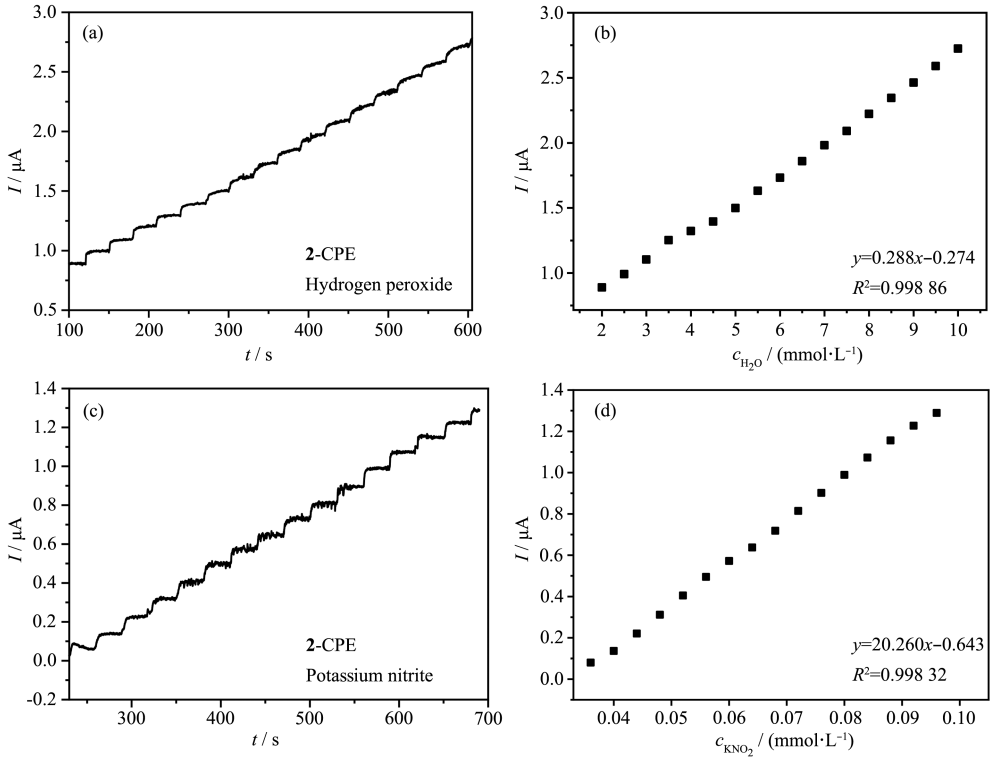

Fig.6 (a, c) Amperometric response for **2**-CPE on successive addition of 0.4 mmol·L^{-1} hydrogen peroxide and potassium nitrite to 0.1 mol·L^{-1} H_2SO_4 + 0.5 mol·L^{-1} Na_2SO_4 aqueous solution; (b, d) Steady-state calibration curve for current versus concentration with applied potential of −400 mV for **2**-CPE

graph at the **2**-CPE. The electrode response was linear for nitrite within the concentration range of 36~96 μmol·L^{-1}, and the sensitivity was 20.26 μA·L·mmol^{-1} (Correlation coefficient: 0.998 32). The detection limit was 0.370 mmol·L^{-1} when the signal-to-noise ratio was 3. Under the same conditions, we also tested the sensing of potassium nitrite by **3**- and **4**-CPEs, as shown in Fig.S8.

In electrochemical sensors, the selectivity plays an important role[30]. In this work, we choose various inorganic ions, such as CO_3^{2-}, HCO_3^-, CH_3COO^-, SO_4^{2-}, Cl^- and Br^-, as possible interferences in the detection of nitrite ions. It can be observed that when 0.1 mol·L^{-1} KNO_2 was added to 0.1 mol·L^{-1} H_2SO_4+0.5 mol·L^{-1} Na_2SO_4 aqueous solution, a significant increase occurred in the amperometric current responses. However, with addition of Na_2CO_3, $NaHCO_3$, Na_2SO_4, NaCl, KCl, KBr and CH_3COONa at the same concentration of NO_2^- to 0.1 mol·L^{-1} H_2SO_4+0.5 mol·L^{-1} Na_2SO_4 aqueous solution at regular intervals, these interfering substances had almost no influence on the amperometric current responses. So, this result suggests that **2**-CPE electrode possesses excellent selectivity towards nitrite ions (Fig.7).

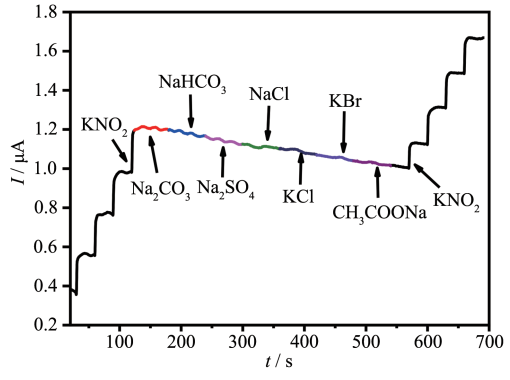

Fig.7 Amperometric current responses of **2**-CPE in aqueous solution upon addition of various inorganic salts

2.5 Photocatalytic properties

Owing to the environmental harm of organic dyes, it is significant to utilize low-cost and easily available

materials for the degradation of dyes[31]. At present, many POM-based compounds have been verified that they can act as photocatalysts to degrade dyes. In this work, cationic dyes methylene blue (MB), gentian violet (GV), methyl orange (MO) and rhodamine B (RhB) were selected to explore the photocatalytic behaviors of compounds **1**~**4** at room temperature under UV irradiation. In the dye adsorption experiment, 50 mg product of the title compound was added into 250 mL aqueous solutions of MB (0.01 mmol·L^{-1}) with magnetically stirred at room temperature under UV irradiation. At regular time intervals of 30 min, 5 mL transparent sample solution was taken out and analyzed on a UV-Vis spectrophotometer. Firstly, we tested the degradation activity of metal-organic subunits and POMs on organic dye MB. As shown in Fig.S9, the photocatalytic activity of MO subunits was very weak. POMs have a certain catalytic degradation activity on MB, but POM-based compounds are more active.

As shown in Fig. 8, the absorption peaks of MB decreased obviously with increasing reactive time for compounds **1**~**4**. The maximum conversions of MB are 34.6% for **1**, 63.3% for **2**, 28.5% for **3** and 46.3% for **4** after 120 min in the presence of compounds **1**~**4**, respectively (Fig. S10). These results suggest that all compounds show photocatalytic properties for MB under UV irradiation, especially compound **2**. Fig. 9 shows that the absorption peaks of GV decreased obviously with increasing reactive time for compounds **1**~**4**. After 120 min, the conversions of GV were 55.8% for **1**, 46.0% for **2**, 40.3% for **3** and 40.9% for **4**, respectively (Fig. S10). In a word, the synergetic effect of POM anions, TMs and organic ligands may induce the distinct photocatalytic effects. Both the types of reactants (POMs, TMs and ligands) and the linking modes may lead different synergetic effect, which may play different photocatalytic effects. However, compounds **1**~**4** almost exhibit no photocatalytic behaviors at room temperature under UV irradiation for MO and RhB.

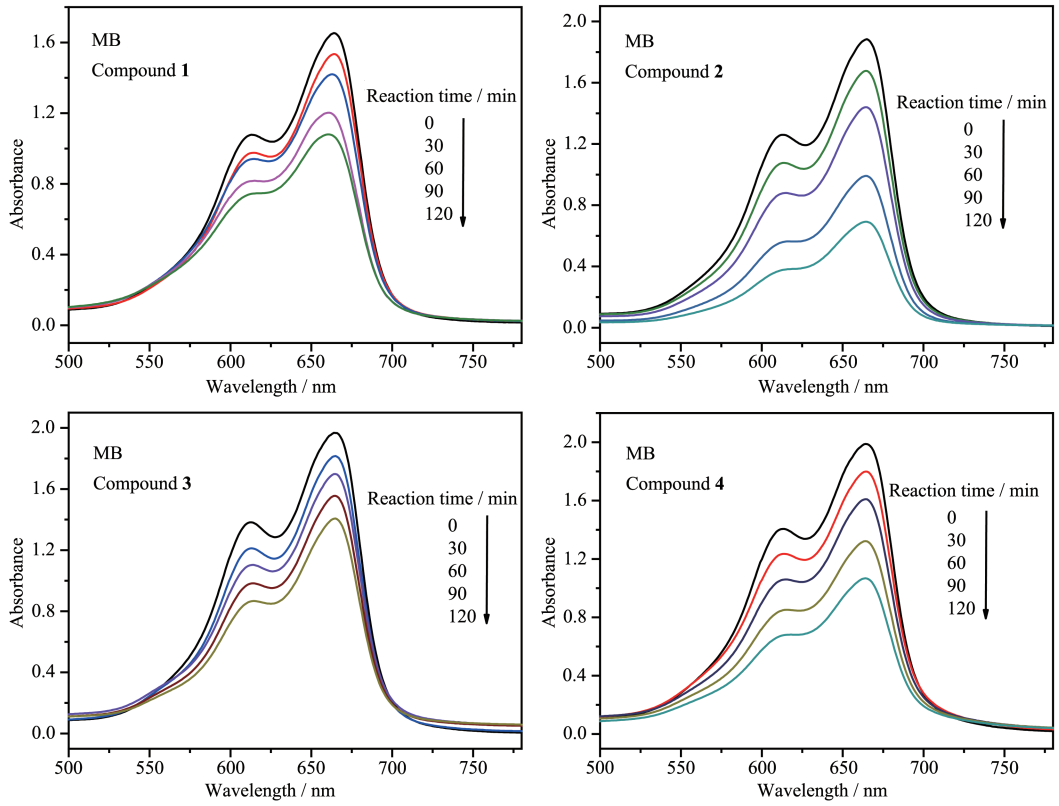

Fig.8　Absorption spectra of MB solution during the decomposition reaction under UV irradiation in the presence of compounds **1**~**4**

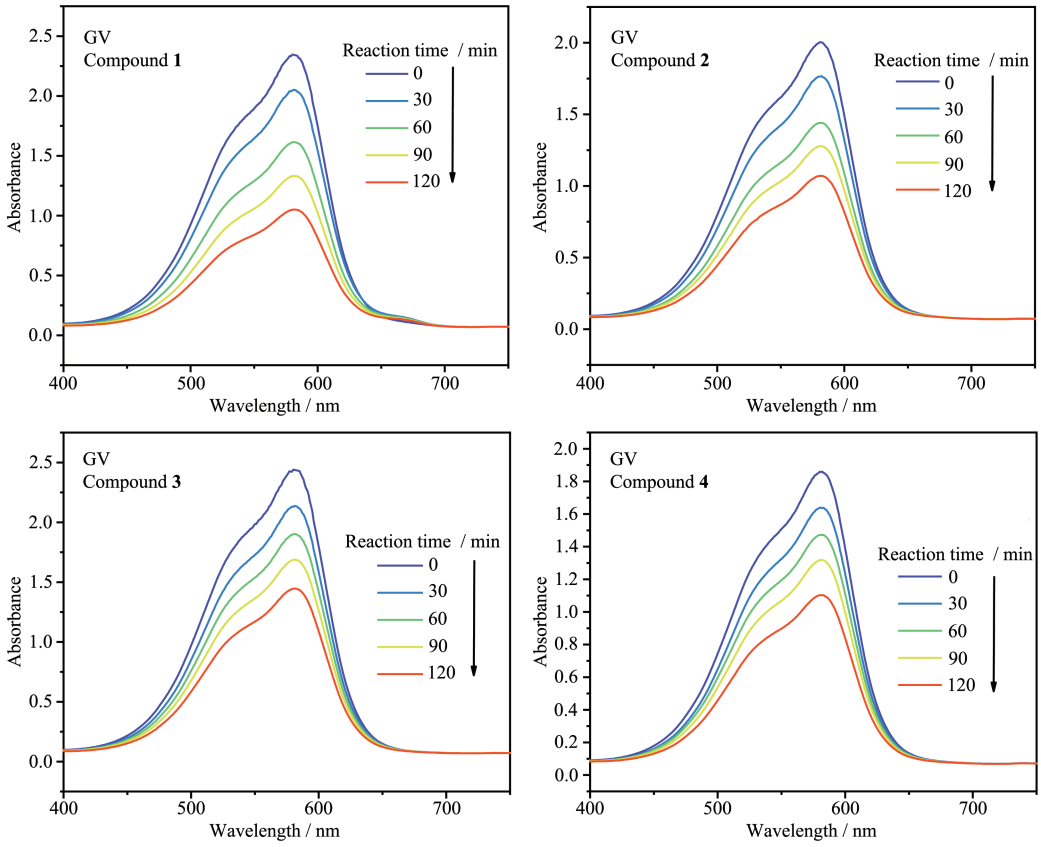

Fig.9 Absorption spectra of GV solution during the decomposition reaction under UV irradiation in the presence of compounds **1~4**

2.6 Selective photocatalytic properties of compounds 1~4

Selective degradation of toxic dyes is more attractive and challenging. Therefore, we chose the cationic dyes MB and MO, MB and RhB with the same charge and different sizes as the model to study the selective degradation ability of the synthesized compounds. Compounds **1~4** were immersed and stirred in an equimolar ratio of MB and MO mixed solution, then the degraded solution was taken out to determine the degradation ability of compounds **1~4** under UV irradiation. As shown in Fig. 10, the results show that the absorption peaks of all MB gradually decreased, while the characteristic absorption peaks of MO exhibited that the degradation rate of MO was relatively small. Furthermore, the graph of selective degradation of dyes clearly shows that the color of the mixed MB-MO solution changed from dark green to pure orange, which was easily observed (Fig. S11). The similar selective degradation of MB was also observed in an equimolar ratio of MB and RhB mixed solution (Fig. 11). This test results exhibit that compounds **1~4** have selective degradation of cationic MB dye in wastewater in some extent. However, the selective degradation property of compound **4** is relatively weak in the mixed MB-MO solution. Though compounds **2**, **3**, **4** are isostructural, their components are different. The different photocatalytic effects may be induced by the synergetic effect of POM anions, TMs and organic ligands.

In order to study the recyclability of compounds **1~4** as catalysts, we recovered the catalyst under the same conditions and repeated the above selective photocatalytic experiments three times. After three cycles, the catalytic degradation rates of MB by compounds **1~4** were almost unchanged (Fig.S12).

2.7 Luminescence sensing functions of Hg^{2+} of compounds 1, 2 and 4

The possible mechanism for the significant quenching effect of Hg^{2+} is that according to Lewis acid-base theory, Hg^{2+} ion (Lewis acid) has a high complex-

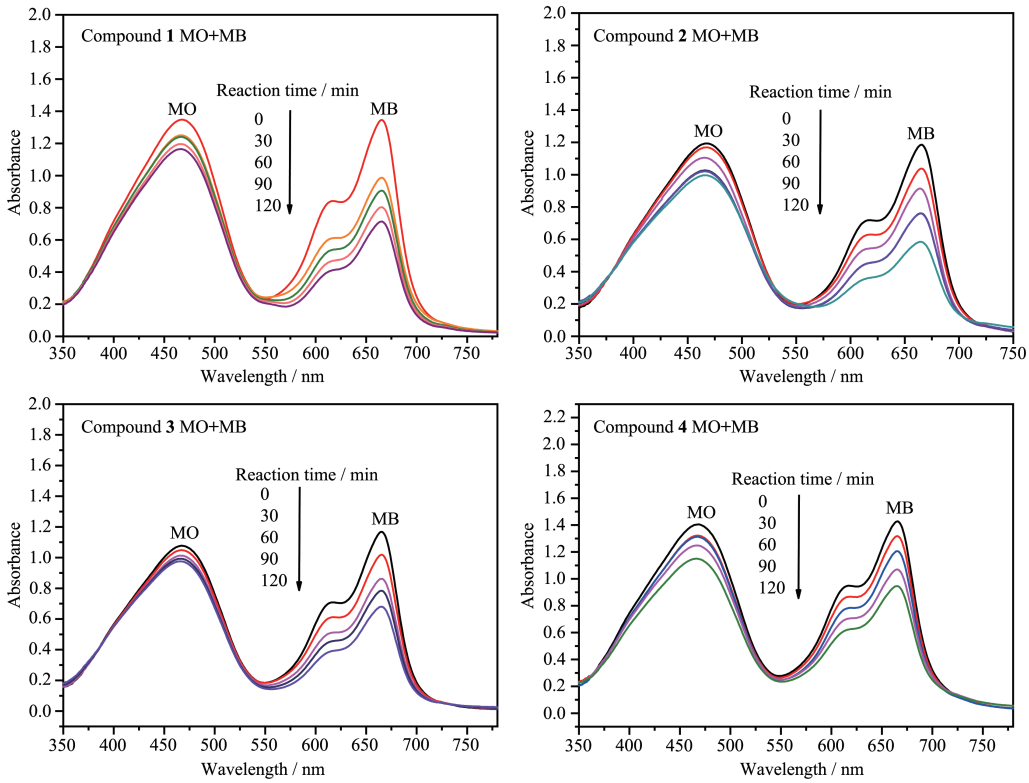

Fig.10　Absorption spectra of MB-MO solution during the decomposition reaction under UV irradiation in the presence of compounds **1~4**

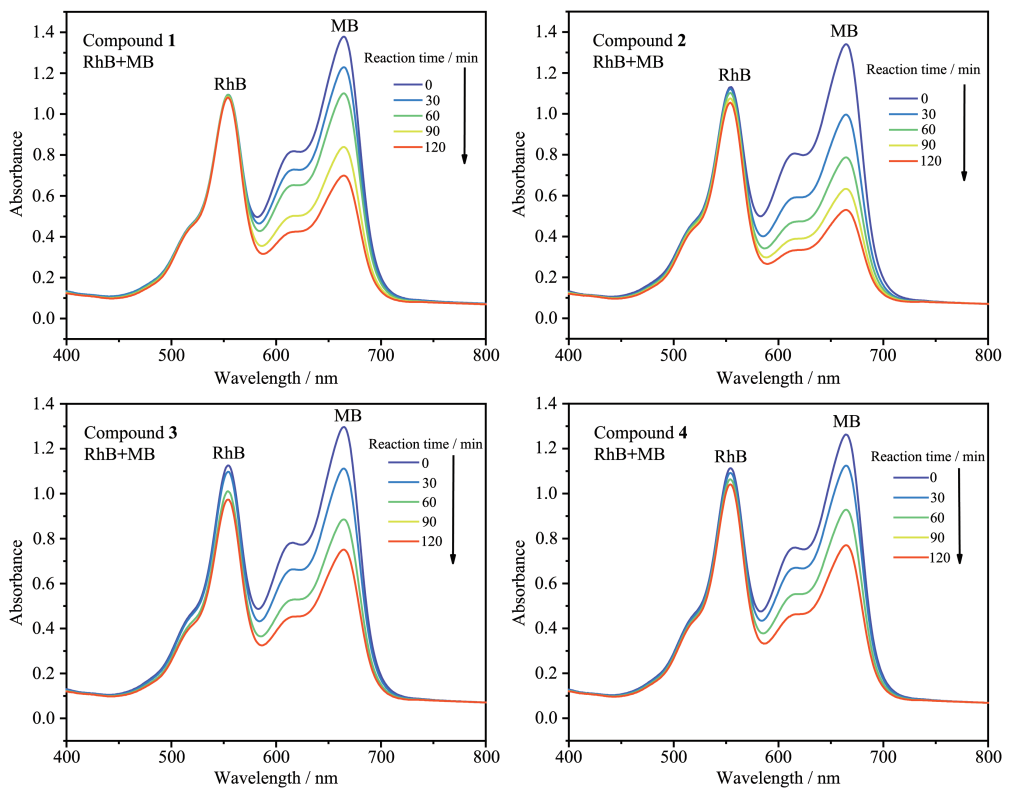

Fig.11　Absorption spectra of MB-RhB solution during the decomposition reaction under UV irradiation in the presence of compounds **1~4**

ation affinity to S atom (Lewis base). This result may decrease the degree of delocalization in these compounds, minimizing the energy-transfer efficiency and resulting in fluorescence quenching[32-35]. The title compounds **1**~**4** also own uncoordinated S atoms. So, we performed the experiments to explore their luminescence sensing functions of Hg^{2+}. However, only compounds **1**, **2** and **4** can act as luminescent probes for Hg^{2+}, while compound **3** cannot be used as a mercury ion sensor. The sensitivity to other ions was not obvious, even for Cd^{2+} (Fig. S13). Thus, in this work, we chose compounds **1**, **2** and **4** as examples to explore their potential sensing functions for Hg^{2+} in suspensions of dichloromethane solution of **1**, **2** and **4** (0.1 g·L^{-1}). The emission spectrum of **1** suspension at room temperature excited at 254 nm showed an intense emission band at 398 nm (Fig.12). The quantitative quenching behavior of **1** was further investigated by adding different concentrations of Hg^{2+} ions ranging from 10 to 80 mmol·L^{-1} to the suspension. It can be observed in Fig.12a that the luminescence intensity of **1** decreased gradually with increasing concentration of Hg^{2+} ions. Fig. 12b shows linearity relationship between the relative intensity and the concentration of Hg^{2+} ions, showing that there was a good linear relationship between 10 and 50 mmol·L^{-1}. The results exhibit that compound **1** can be regarded as a reliable and efficient luminescent sensor to detect Hg^{2+} ions. In order to gain a further understanding of this phenomenon, we have performed the same experiments by introducing Ni^{2+}, Zn^{2+}, Cd^{2+}, Co^{2+}, Cu^{2+} and Fe^{3+} to the system. With the addition of the other ions (80 mmol·L^{-1}) to the suspen-

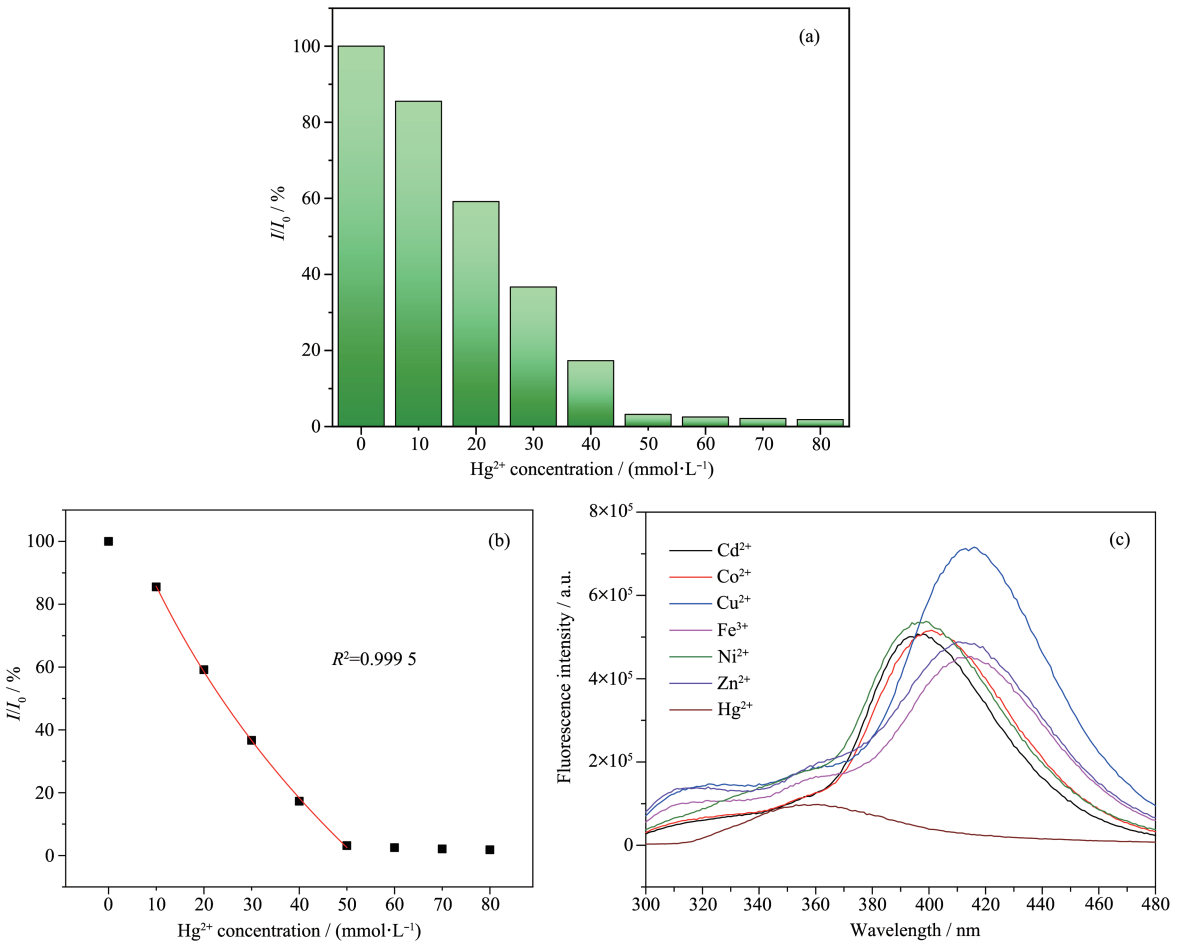

I_0: fluorescence intensity without Hg^{2+}; I: fluorescence residual intensity with adding different Hg^{2+} concentrations

Fig.12 (a) Fluorescence intensity of **1** with gradually increased Hg^{2+}; (b) I/I_0 vs Hg^{2+} concentration showing a fluorescence change after adding Hg^{2+}; (c) Emission spectra (excited at 254 nm) of **1** suspension with the addition of different metal ions with concentration of 80 mmol·L^{-1}

sion of **1**, the decreasing degree of the luminescence intensities was not obvious compared with Hg^{2+} (Fig. 12c). The same phenomenon happened on compounds **2** and **4**. Namely, the introduction of Hg^{2+} decreased the luminescence intensities of **2** and **4**. And on increasing the Hg^{2+} concentration up to 80 mmol·L^{-1}, the luminescence intensities changed to the lowest level (Fig. 13a, Fig. S14a) and there was a good linear relationship between 30 and 60 mmol·L^{-1} for **2** and between 10 and 50 mmol·L^{-1} for 4 (Fig.13b, Fig.S14b). Although the luminescence intensities decreased by the introduction of other equal Ni^{2+}, Zn^{2+}, Cd^{2+}, Co^{2+}, Cu^{2+} and Fe^{3+}, the luminescence intensities were still much stronger than that of Hg^{2+} (Fig.13c, Fig.S14c).

In our experiments, it was found that as the concentration of Hg^{2+} increased, the fluorescence intensity decreased while the peak position also changed, from 398 nm to 353 nm. This is due to the coordination of Hg^{2+} with the S atom in ligand L, forming a new charge transfer.

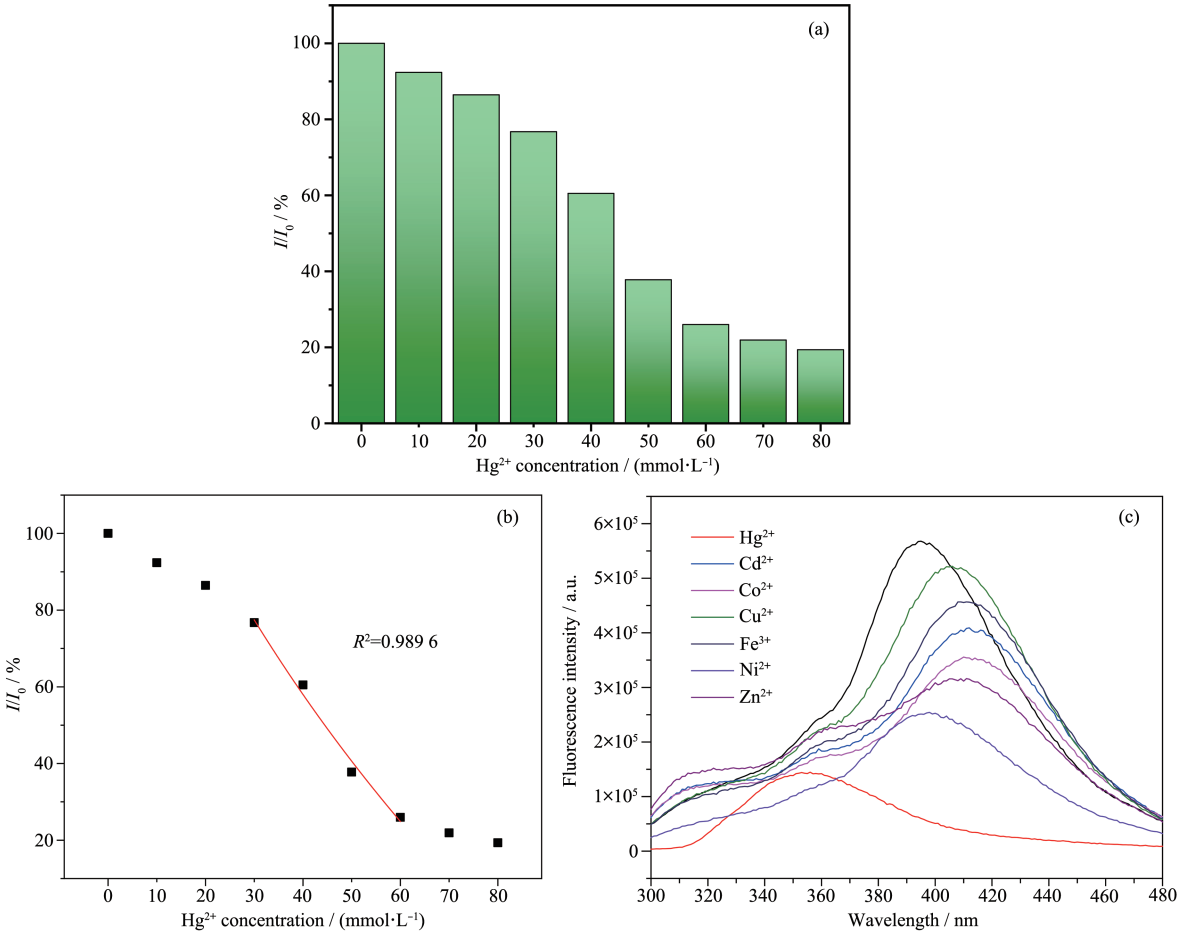

I_0: fluorescence intensity without Hg^{2+}; I: fluorescence residual intensity with adding different Hg^{2+} concentrations

Fig.13　(a) Fluorescence intensity of **2** with gradually increased Hg^{2+}; (b) I/I_0 vs Hg^{2+} concentration showing a fluorescence change after adding Hg^{2+}; (c) Emission spectra (excited at 254 nm) of **2** suspension with the addition of different metal ions with concentration of 80 mmol·L^{-1}

3　Conclusions

In this work, by using a flexible S-containing ligand L, we have synthesized four Keggin-based compounds **1~4** under hydrothermal conditions. Compound **1** exhibits a 2D layer with tri-nuclear Cu(I) cycles linked by anions, while isostructural compounds **2~4** show 1D chains with tetra-nuclear cycles $[Cu_4L_6]^{4+}$ connected by POM anions. Compounds **1~4** exhibit good electrochemical and selective photocatalytic proper-

ties. In addition, compounds **1**, **2** and **4** suspensions exhibit good luminescence recognition for Hg^{2+}. Further study will focus on design and syntheses of other POM-based compounds containing S donors as Hg^{2+} fluorescent probes.

Acknowledgements: The financial supports of this research included the National Natural Science Foundation of China (Grants No. 21571023, 21101015), Liaoning Revitalization Talents Program (Grant No.XLYC1807049) and the General Program Fund for Education Department of Liaoning Province (Grants No. LQ2020010, LJ2019006), which are gratefully acknowledged.

Supporting information is available at http://www.wjhxxb.cn

References:

[1] Yu L, Du X Q, Ding Y, et al. *Chem. Commun.*, **2015**,**51**(98):17443-17446

[2] Liu Y, Zhao S F, Guo S X, et al. *J. Am. Chem. Soc.*, **2016**,**138**(8):2617-2628

[3] Li S B, Zhang L, Lan Y Q, et al. *Chem. Commun.*, **2018**,**54**(16):1964-1967

[4] Proust A, Matt B, Villanneau R, et al. *Chem. Soc. Rev.*, **2012**,**41**(22):7605-7622

[5] Walsh J J, Bond A M, Forster R J, et al. *Coord. Chem. Rev.*, **2016**,**306**(1):217-234

[6] Zhang C, Bu W B, Ni D L, et al. *J. Am. Chem. Soc.*, **2016**,**138**(26):8156-8164

[7] Wang X L, Zhang R, Wang X, et al. *Inorg. Chem.*, **2016**,**55**(13):6384-6393

[8] Liu J Y, Ma C B, Chen H, et al. *CrystEngComm*, **2015**,**17**(45):8736-8745

[9] Ibrahim M, Mereacre V, Leblanc N, et al. *Angew. Chem. Int. Ed.*, **2015**,**54**(51):15574-15578

[10]AlDamen M A, Juan J M C, Coronado E, et al. *J. Am. Chem. Soc.*, **2008**,**130**(28):8874-8875

[11]Arefian M, Mirzaei M, Eshtiagh-Hosseini H, et al. *Dalton Trans.*, **2017**,**46**(21):6812-6829

[12]Bloch W M, Holstein J J, Hiller W, et al. *Angew. Chem. Int. Ed.*, **2017**,**56**(28):8285-8289

[13]Salomon W, Riviere E, Lopez X, et al. *Dalton Trans.*, **2018**,**47**(31):10636-10645

[14]Jiao Y Q, Qin C, Zang H Y, et al. *CrystEngComm*, **2015**,**17**(10):2176-2189

[15]Tian A X, Hou X, Ying Y, et al. *RSC Adv.*, **2015**,**5**(66):53757-53765

[16]Taleghani S, Mirzaei M, Eshtiagh-Hosseini H, et al. *Coord. Chem. Rev.*, **2016**,**309**:84-106

[17]Ying J, Liu J N, Li T T, et al. *J. Coord. Chem.*, **2017**,**70**(7):1146-1155

[18]Tian A X, Ning Y L, Ying J, et al. *CrystEngComm*, **2015**,**17**(29):5569-5578

[19]Tian A X, Ji X B, Sun N, et al. *J. Chem. Crystallogr.*, **2016**,**47**(1):1-9

[20]Pearson R G. *J. Am. Chem. Soc.*, **1963**,**85**(22):3533-3539

[21](a)Sheldrick G M. *Acta Crystallogr. Sect. A*, **2008**,**A64**(1):112-122

(b)Sheldrick G M. *SHELXS*-97, University of Göttingen, Germany, 1997.

[22]Dolomanov O V, Bourhis L J, Gildea R J, et al. *J. Appl. Crystallogr.*, **2009**,**42**(2):339-341

[23]Brown I D, Altermatt D. *Acta Crystallogr. Sect. B*, **1985**,**B41**:244-247

[24]Wang X L, Qin C, Wang E B, et al. *Chem. Commun.*, **2007**,**41**:4245-4247

[25]Liu C M, Zhang D Q, Zhu D B. *Cryst. Growth Des.*, **2002**,**6**(2):524-529

[26](a)Rocchiccioli-Deltcheff C, Thouvenot R, Franck R. *Spectrochim. Acta*, **1976**,**32**(3):587-597

(b)Rocchiccioli-Deltcheff C, Fournier M, Franck R, et al. *Inorg. Chem.*, **1983**,**22**(2):207-216

[27]Sha J Q, Peng J, Zhang Y, et al. *Cryst. Growth Des.*, **2009**,**9**(4):1708-1715

[28](a)Tian A X, Lin X L, Liu Y J, et al. *J. Coord. Chem.*, **2012**,**65**(12):2147-2158

(b)Sadakane M, Steckhan E. *Chem. Rev.*, **1998**,**98**(1):219-237

[29]Dong B X, Bu F Y, Wu Y C, et al. *Cryst. Growth Des.*, **2017**,**17**(10):5309-5317

[30]Mani V, Periasamy A P, Chen S M. *Electrochem. Commun.*, **2012**,**17**:75-78

[31]Wang X L, Chang Z H, Lin H Y, et al. *Dalton Trans.*, **2014**,**43**(32):12272-12278

[32]Zhao Q, Cao T Y, Li F Y, et al. *Organometallics*, **2007**,**26**(8):2077-2081

[33]Liu Y, Li M Y, Zhao Q, et al. *Inorg. Chem.*, **2011**,**50**(13):5969-5977

[34]Tian A X, Ning Y L, Yang Y, et al. *Dalton Trans.*, **2015**,**44**(37):16486-16493

[35]Tian A X, Yang M L, Fu Y B, et al. *Inorg. Chem.*, **2019**,**58**(7):4190-4200